Crossover between Bulk and Interface Photovoltaic Mechanisms in a Ferroelectric Vertical Heterostructure

Amr Abdelsamie,[1] Lu You,[2,*] Le Wang,[1,‡] Shuzhou Li,[1] Mingqiang Gu,[3] and Junling Wang[1,3,†]

[1] *School of Materials Science and Engineering, Nanyang Technological University, Singapore 639798, Singapore*

[2] *Jiangsu Key Laboratory of Thin Films, School of Physical Science and Technology, Soochow University, 1 Shizi Street, Suzhou 215006, China*

[3] *Department of Physics, Southern University of Science and Technology, Shenzhen 518055, China*

(Received 25 October 2021; revised 12 January 2022; accepted 19 January 2022; published 16 February 2022)

The bulk photovoltaic (BPVE) effect in crystals lacking inversion symmetry offers great potential for optoelectronic applications due to its unique properties, such as above-band-gap photovoltage and switchable photocurrent. Because of their large spontaneous polarizations, ferroelectric materials are ideal platforms for studying the BPVE. However, identifying the origin of an experimentally observed photovoltaic response is often challenging due to the entanglement between bulk and interface effects, leading to much debate in the field. This issue is particularly pronounced in vertical heterostructures, where the two effects are comparable. Here, we report crossover between bulk- and interface-dominant responses in vertical $BiFeO_3$ heterostructures when changing the photon energy. We show that well-above-band-gap excitation leads to a bulk photovoltaic response, but band-edge excitation requires interface band bending to separate the photocarriers. Our findings not only help to clarify contradicting reports in the literature, but also lay the foundation for a deeper understanding of the ferroelectric photovoltaic effect and its applications in various devices.

DOI: 10.1103/PhysRevApplied.17.024047

I. INTRODUCTION

The bulk photovoltaic effect (BPVE), which occurs in noncentrosymmetric crystals, such as ferroelectrics, is one of the most striking manifestations of nonlinear optical phenomena [1]. Under uniform illumination, a photocurrent (or photovoltage) is induced in otherwise spatially homogeneous crystals by taking advantage of the crystal asymmetry to separate photoexcited electron-hole (*e*-*h*) pairs [Fig. 1(a)] [2–4]. The photocurrent is generated throughout the active layer and an above-band-gap photovoltage can be achieved, unlike in conventional junction-based photovoltaics [5–7]. Thus, solar cells based on the BPVE are promising alternatives to overcome the Shockley-Queisser (SQ) efficiency limit [8]. However, it is generally accepted that Schottky barriers at the ferroelectric-metal interfaces can also lead to charge separation [Figs. 1(b) and 1(c)] [9–11]. In both cases, photovoltaic responses in ferroelectric based cells are bidirectional, following polarization reversal [Fig. 1(d)] [12–15]. Furthermore, it is argued that ferroelectric domain walls (DWs) may act as photoelectromotive sources to separate (*e*-*h*) pairs [5,16,17] or introduce an additional conduction path [18,19].

One fingerprint of the BPVE is the angular dependence of photovoltaic response on light polarization [4,20]. This property, in turn, is exploited to distinguish the BPVE from the conventional one. To date, most of the studies are carried out on ferroelectrics in either single-crystal form [2,21,22] or thin films with coplanar electrodes [17,23–25]. In these geometries, the active-layer size is very large, diminishing the impact of the interface Schottky barrier on the total photovoltaic output. However, vertical heterostructures are much more relevant to applications. In this case, the interface depletion region would be comparable in dimensions to the ferroelectric layer thickness. There is a large volume of studies concluding that photovoltaic response in vertical heterostructures is dominated by interface band bending [12,14,26–28], and tuning the interface properties controls the overall photovoltaic response in some cases [29,30]. However, there also exists a number of reports on the BPVE in vertical heterostructures comprising $BiFeO_3$ [31], $BaTiO_3$ [32,33], and $BiVO_4$ [34], where contributions from interfaces or the tensorial nature of the BPVE are not thoroughly examined. Therefore, clarifying the dominating photovoltaic mechanism in vertical ferroelectric heterostructures is of crucial importance for both fundamental studies and practical applications.

*lyou@suda.edu.cn

†jwang@sustech.edu.cn

‡Present address: Physical and Computational Sciences Directorate, Pacific Northwest National Laboratory, Richland, Washington 99354, USA.

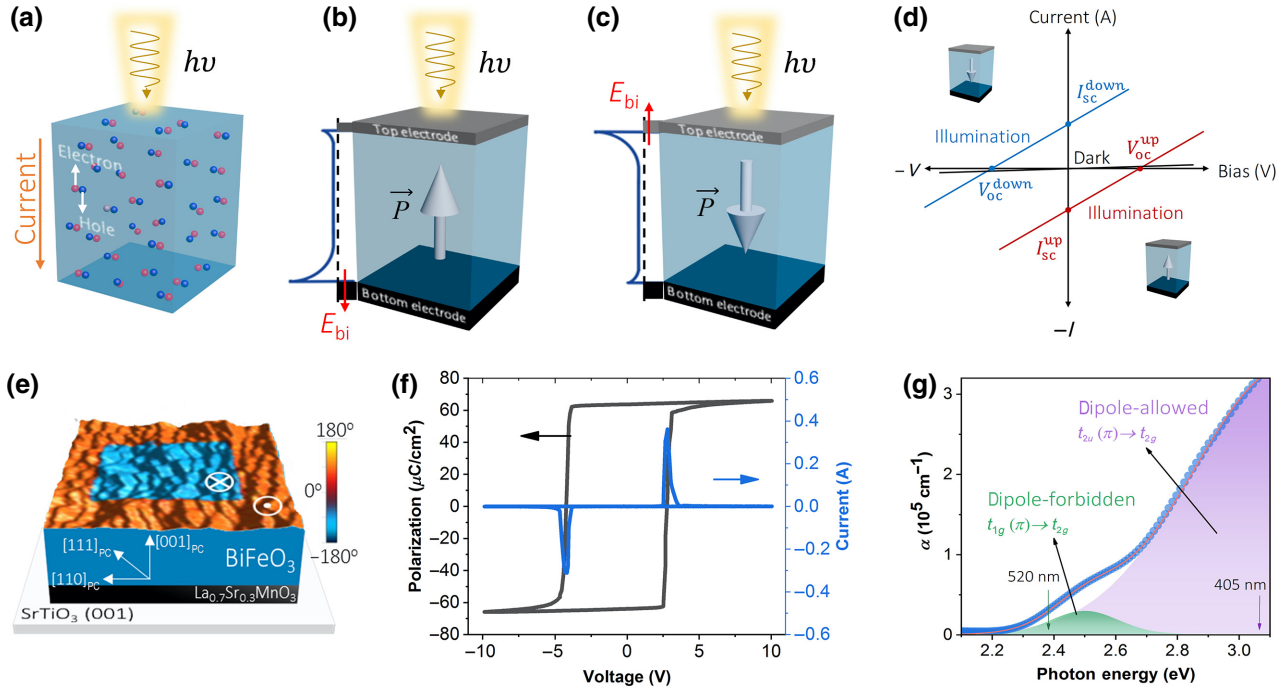

FIG. 1. Photovoltaic effects in ferroelectric materials and characteristics of the $BiFeO_3$ films used in this study. (a) Photogenerated electron-hole pairs in noncentrosymmetric crystals are separated in the homogeneous bulk, yielding the bulk photovoltaic effect. However, bringing metallic electrodes (gray and black layers) in contact with the ferroelectric material creates Schottky barriers. Switching the ferroelectric polarization, $\vec{P}$, from (b) up state to (c) down state modulates the Schottky barrier heights at the top and bottom interfaces. Electronic band structure is depicted on the left-hand side of the device (dashed line represents Fermi level). Photoexcited charge carriers are separated at the interface. (d) Reversal of ferroelectric polarization flips the photocurrent between negative and positive directions. (e) Piezoresponse-force-microscopy phase image overlaid on the topography of $BiFeO_3$ film with as-grown and switched areas. (f) Polarization-voltage and switching-current curves of the $Pt/BiFeO_3/La_{0.7}Sr_{0.3}MnO_3$ capacitor. (g) Measured absorption coefficient of $BiFeO_3$, revealing the weak dipole-forbidden charge-transfer (CT) transition with onset at 2.2 eV and the strong dipole-allowed CT transition above the nominal band gap of 2.7 eV. Purple and green arrows point to the laser energies used in this study.

Bismuth ferrite ($BiFeO_3$) offers an ideal platform to investigate the ferroelectric photovoltaic effect. It crystallizes in the rhombohedral space group $R3c$ [pseudocubic (PC) lattice parameters $a_{PC} = 3.965$ Å, $\alpha_{PC} = 89.4°$] and possesses spontaneous polarization along the $[111]_{PC}$ direction (remnant polarization, P_r, $\sim 100\ \mu C\,cm^{-2}$) [35]. In this study, we aim to clarify the dominating mechanism of the photovoltaic response in vertical $BiFeO_3$ capacitors by exploiting linearly polarized light. It is shown that $BiFeO_3$ exhibits uniaxial optical anisotropy, which coincides with the polar axis, i.e., $[111]_{PC}$. In other words, linearly polarized light would undergo anisotropic absorption in $BiFeO_3$ [36–38], which will be taken into consideration. Furthermore, single-domain $BiFeO_3$ thin films are used to exclude the impact of domain walls.

II. EXPERIMENTS

A. Heterostructure preparation

Our device consists of a 500-nm $(001)_{PC}$-oriented $BiFeO_3$ film sandwiched between $La_{0.7}Sr_{0.3}MnO_3$ (10 nm, bottom electrode) and Pt (10 nm, top electrode). $BiFeO_3$ and $La_{0.7}Sr_{0.3}MnO_3$ are epitaxially grown using the pulsed laser deposition technique. To obtain a single-domain state, the films are deposited on (001)-oriented $SrTiO_3$ substrates with a 4° miscut towards the $\langle 110\rangle_{PC}$ direction [39]. For the absorption measurements, two-side-polished $SrTiO_3$ substrates are used. Stoichiometric targets are ablated by a KrF excimer laser (248 nm). The growth parameters are summarized in Table I. Following deposition, arrays of 40×40-μm^2 Pt electrodes are sputtered on top of $BiFeO_3$ films through a shadow mask at room temperature.

B. Device characterization

A ferroelectric tester (Precision Multiferroic, Radiant Technologies) is used to measure the ferroelectric hysteresis loop at 1 kHz. Local polarization mapping and switching are performed using a piezoelectric force microscope (Asylum Research MFP-3D) with Pt/Ir-coated tips.

TABLE I. Growth conditions for $BiFeO_3$ and $La_{0.7}Sr_{0.3}MnO_3$.

Thin film	Substrate temperature (°C)	Oxygen pressure (mTorr)	Repetition rate (Hz)	Fluence (J cm^{-2})	Thickness (nm)
$BiFeO_3$	650	50	10	1.2	500
$La_{0.7}Sr_{0.3}MnO_3$	800	200	3	2	10

The *I-V* data are collected by using a pA-meter–direct-current (dc) voltage source (Hewlett Package 4140B) on a low-noise probe station. To illuminate the cell, lasers with wavelengths of 405 nm (approximately 0.65 W cm^{-2}) and 520 nm (approximately 0.19 W cm^{-2}) are used. White light is provided by a halogen lamp with an intensity of about 0.05 W cm^{-2}. A Glan-Thomson calcite polarizer is placed between the objective lens and the light source to obtain linearly polarized light.

C. Linear dichroism in $BiFeO_3$

The optical absorption of $BiFeO_3$ films is determined using a Perkin Elmer Lambda 950 ultraviolet-to-visible (UV-vis) spectrophotometer. $BiFeO_3$ films (170 nm) are directly grown on two-side-polished $SrTiO_3$ substrates to ensure transparency. All curves are collected for wavelengths between 400 and 600 nm at room temperature. It should be noted that accurate data for wavelengths shorter than 400 nm cannot be obtained due to substrate absorption. Data are deduced from absorbance spectra after removing contributions from the $SrTiO_3$ substrate. To study the absorption of $BiFeO_3$ films for linearly polarized light, the spectrometer is equipped with a Glan-Thomson calcite polarizer (resembling the one used to measure the photovoltaic performance). Moreover, the sample is mounted on a rotatable stand to enable rotation between $-90°$ and $+90°$ while ensuring a constant light intensity.

III. RESULTS

A. Characterizing ferroelectric and optical properties

Prior to the photovoltaic measurements, we first assess the basic ferroelectric and optical properties of the $BiFeO_3$ active layer. $BiFeO_3$ exhibits a single-ferroelectric-domain structure, which is confirmed by piezoelectric force microscopy, as shown in Fig. 1(e). The $BiFeO_3$ is single phase with a *c*-axis lattice constant of 3.978 Å. Figure 1(f) presents the ferroelectric hysteresis loop and transient-current curve. The rectangular shape of the loop reflects the intrinsic and monodomain ferroelectricity of the $BiFeO_3$ film with a remnant polarization of $P_r = 65\ \mu C\ cm^{-2}$ along the $[001]_{PC}$ direction. The optical absorption spectrum of the $BiFeO_3$ film [Fig. 1(g)] shows a direct gap at about 2.7 eV (approximately 460 nm), as plotted in Fig. S1 within the Supplemental Material [40], which is attributed to the $t_{2u}(\pi) \rightarrow t_{2g}(\pi^*)$ dipole-allowed O 2*p* to Fe 3*d* CT transition [36,41–43]. It also displays a weak yet distinct absorption peak with the onset at about 2.2 eV (approximately 560 nm), which is usually assigned to the $t_{1g}(\pi) \rightarrow t_{2g}(\pi^*)$ dipole-forbidden CT transition. This low-lying electronic structure is widely reported in $BiFeO_3$ samples in various forms and by different synthesis methods, and it appears to be a common feature of CT ferrite insulators with low-symmetry FeO_6 octahedra distortions, signifying the intrinsic nature of this transition [43]. Furthermore, due to the strong electron-phonon coupling, the sub-band-gap transition results in local lattice deformation, and thus, the formation of self-trapped excitonic states [44,45], which also underlies the previously reported ultrafast photostriction [46,47] and broadband photoluminescence emission [48] of $BiFeO_3$.

B. Light-polarization-angle-dependent photocurrents

Photovoltaic measurements are performed on Pt/$BiFeO_3$/$La_{0.7}Sr_{0.3}MnO_3$ devices using linearly polarized light. Here, 405-nm (approximately 3.1-eV) and 520-nm (approximately 2.4-eV) lasers with maximum intensities of 0.65 and 0.19 W cm^{-2}, respectively, and a halogen lamp (maximum intensity of 0.05 W cm^{-2}) are used as the light sources. The sample is first poled into up- or down-state polarization. The sample is illuminated through the top electrode (the thin Pt electrode allows 37%, 32%, and 23% of the 405 nm, 520 nm, and white light, respectively, to pass through). As plotted in Fig. 2(a), light polarization makes an angle θ relative to the in-plane ferroelectric polarization (P_{IP}) of $BiFeO_3$, i.e., $[110]_{PC}$. Hence, $\theta = 0°$ indicates light polarization that is parallel to the in-plane ferroelectric polarization. The out-of-plane photovoltaic behavior is measured for different azimuthal angles of light polarization (from $-90°$ to $+90°$). The short-circuit (SC) currents in both polarization-up and -down states are shown in Figs. 2(b) and 2(c) (more data and further discussion can be found in the Supplemental Material [40]).

Interestingly, modulation of the photocurrents with respect to θ is observed for both 405-nm (in purple) and 520-nm (in green) light, but in completely opposite manners. Under 405-nm illumination, the photocurrent exhibits sinusoidal behavior with its maximum at $\theta = 0°$ and minimum at $\theta = \pm 90°$, which even flips its direction to the up state. In contrast, when illuminating the device with a 520-nm laser, the photocurrent direction remains negative for the up state and positive for the down state across all angles, and contrarily, the sinusoidal photocurrent is maximized at $\theta = \pm 90°$. Unlike 405-nm excitation,

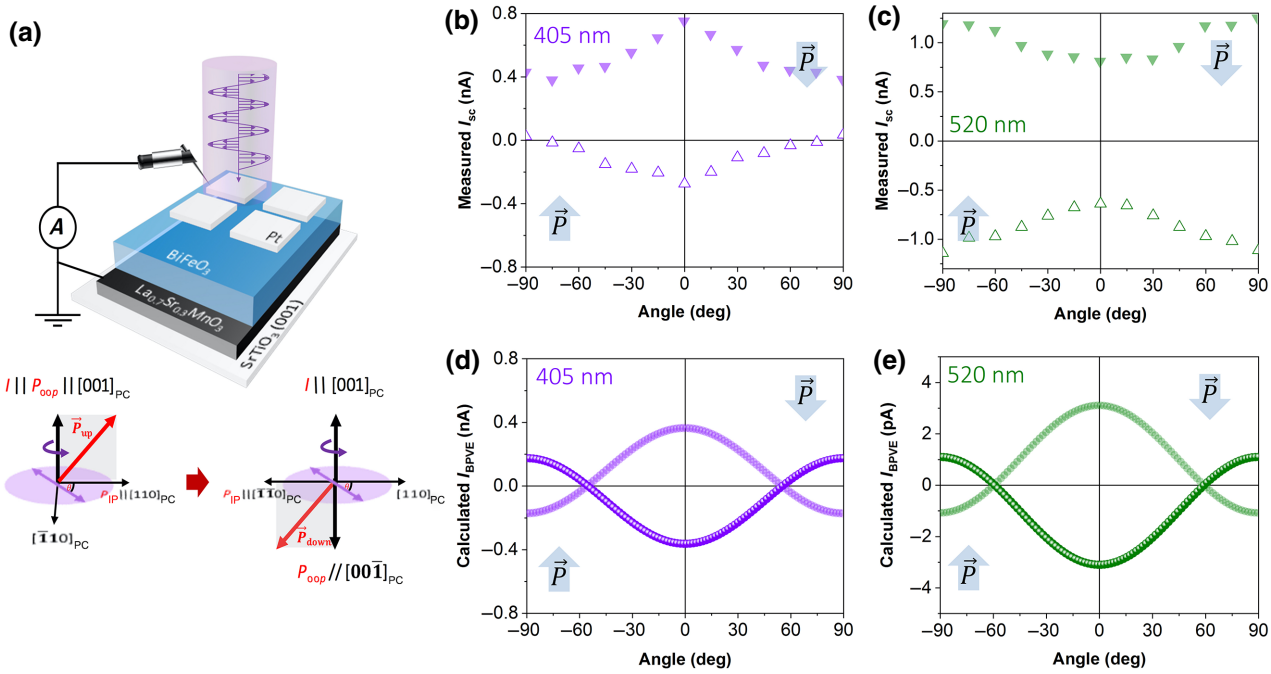

FIG. 2. Light-polarization-dependent photovoltaic response of vertical $Pt/BiFeO_3/La_{0.7}Sr_{0.3}MnO_3$ capacitors. (a) Schematic diagram of the experimental setup (upper panel). Light-polarization angle θ is defined with respect to the in-plane ferroelectric polarization of the sample (i.e., $[110]_{PC}$). In our device, applying voltage above coercivity switches the polarization by 180°, which means that θ remains the same with respect to the in-plane ferroelectric component (bottom panel). Modulation of photocurrents in polarization-up and -down states collected under (b) 405-nm (approximately 3.1-eV) and (c) 520-nm (approximately 2.4-eV) excitations. Calculated I_{BPVE} under (d) 405-nm (approximately 3.1-eV) and (e) 520-nm (approximately 2.4-eV) excitations using Eq. (1).

the 520-nm case shows an almost symmetrical photocurrent response for opposite polarization states. The results suggest that (i) there is a strong correlation between the photovoltaic response and angle θ, and (ii) different photovoltaic mechanisms may be at work for different photon energies.

It is established that BPVE is described by a tensor of third order [4]. In particular, when illuminating $(001)_{PC}$-oriented $BiFeO_3$ crystal, the bulk photocurrent is given by (details in Sec. II)

$$J^{h\upsilon}_{[001]}(\theta) = \frac{I_{opt}}{3\sqrt{3}}\left[A + B\sin\left(2\theta + \frac{\pi}{2}\right)\right], \qquad (1)$$

where $J^{h\upsilon}_{bulk}$ is the photocurrent density along the $[001]_{PC}$ direction under $h\upsilon$ illumination, I_{opt} is the light intensity, A and B are functions of photovoltaic tensor β_{ij} of $BiFeO_3$, and θ is the angle between light polarization and P_{IP} of $BiFeO_3$. We then calculate $I^{405\text{ nm}}_{[001]}$ and $I^{520\text{ nm}}_{[001]}$, in which β_{ij} values are extracted from experimental work on $BiFeO_3$ thin films with coplanar configurations, i.e., from measured bulk photocurrents, as listed in Table II in the Appendix (taken from Ref. [25]). Apparently, the calculated bulk photocurrent under 405-nm light [Fig. 2(d)] reveals a trend (sinusoidal shape) and magnitude coinciding with the experimental result shown in Fig. 2(b), although a large vertical shift is evident for the polarization-down state. In contrast, the photocurrent under a 520-nm laser reveals a trend totally opposite to that described by Eq. (1), and the I_{SC} value is orders of magnitude larger than that calculated for the BPVE. However, it can nonetheless be fitted by a sinusoidal function. Furthermore, linearly polarized white light (generated by a halogen lamp) yields similar behavior to that of 520-nm laser (Supplemental Material [40]).

The apparent opposite behavior suggests that the governing photovoltaic mechanisms for 405- and 520-nm light are likely to be different. While 405-nm light likely

TABLE II. Bulk photovoltaic tensor elements of $BiFeO_3$ at 405 nm (3.1 eV) and 520 nm (2.4 eV). Taken from Ref. [25].

Light source (nm)	β_{15} (V^{-1})	β_{22} (V^{-1})	β_{31} (V^{-1})	β_{33} (V^{-1})
405 (3.1 eV)	8.1×10^{-5}	-1.1×10^{-5}	6.4×10^{-5}	-1.1×10^{-4}
520 (2.4 eV)	3.0×10^{-6}	-4.4×10^{-7}	1.6×10^{-6}	-4.4×10^{-6}

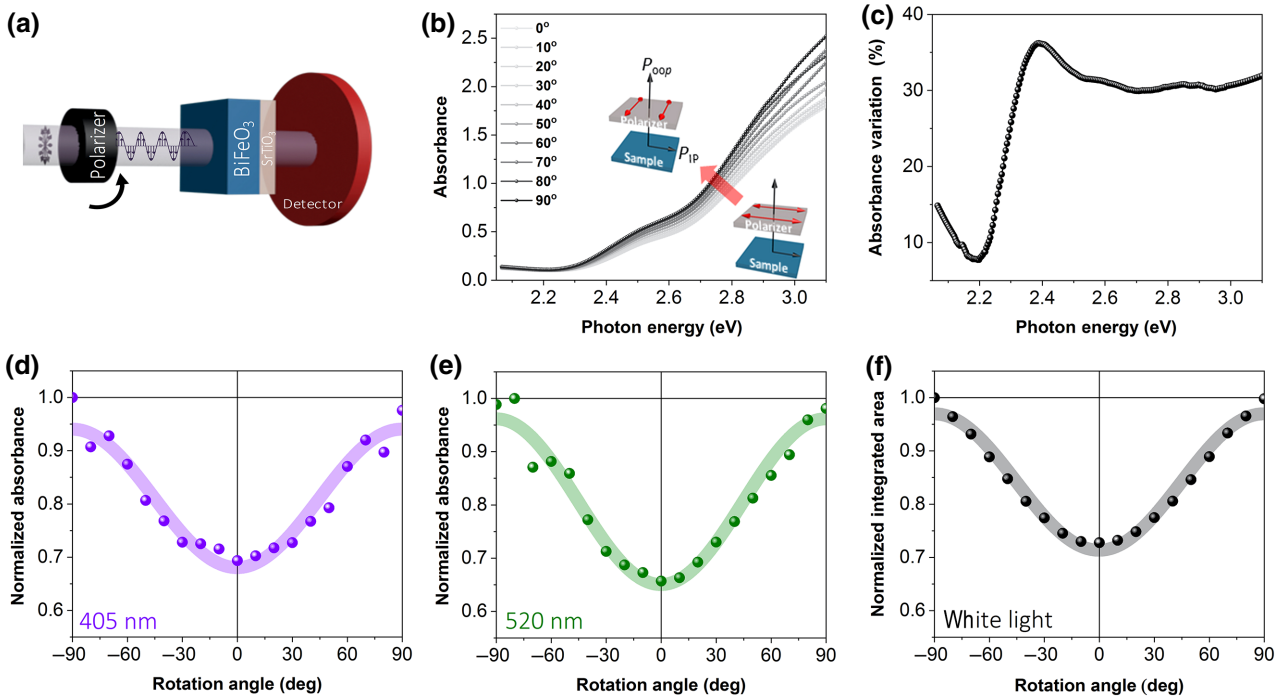

FIG. 3. Angle-dependent polarized-light absorption spectra of $BiFeO_3$ on $SrTiO_3$. (a) Schematic of the measurement setup. (b) Polarized-light absorption spectra collected from 0° to +90°. (c) Photon-energy-dependent absorbance variation, $[A(90°) - A(0°)/A(90°)]\%$, between two orthogonal light polarizations. Extracted angle-dependent absorption at (d) 405 nm and (e) 520 nm, and (f) total integrated area under the absorption curves representing linear dichroism for white light.

generates the BPVE, what is causing the sinusoidal photocurrent under 520-nm illumination? One possibility is the anisotropic light absorption of $BiFeO_3$ [49]. We thus measure the light-polarization-dependent absorption of monodomain $BiFeO_3$ films using a UV-vis spectrophotometer to evaluate the absorption anisotropy quantitatively.

C. Optical linear dichroism of $BiFeO_3$ films

Figure 3 displays the light-polarization-dependent absorption of a $BiFeO_3$ film for $0° < \theta < 90°$. As shown in Fig. 3(c), the percentage of variation between the minimum and maximum absorptions, given by $[A(90°) - A(0°)/A(90°)]\%$, exhibits a positive value over the whole energy range. This indicates that the absorption reaches a maximum when the light and ferroelectric polarizations are orthogonal, and a minimum when they are parallel. To correlate the anisotropic absorption with the photovoltaic response, the angle-dependent absorptions at 405 nm and 520 nm are extracted [Figs. 3(d) and 3(e)], which reveal angular modulation of around 33% and 36%, respectively. Furthermore, the angle-dependent integrated area under the absorption curves is also plotted in Fig. 3(f), representing white-light-absorption anisotropy in $BiFeO_3$ (percentage of modulation approximately 29%). The light-polarization dependence can be fitted by

$$\text{absorption} = a + b\sin\left(2\theta - \frac{\pi}{2} + \varphi\right), \qquad (2)$$

where a and b are positive constants and φ accounts for experimental error in the rotation angle.

It is shown that, when light polarization is set along the $[110]_{PC}$ direction of $(001)_{PC}$-oriented $BiFeO_3$, the optical absorption is at its minimum. The optical excitation increases as the rotation angle increases, and the strongest absorption occurs at light polarization perpendicular to the $[110]_{PC}$ direction. The absorption anisotropy is consistent with the band structure of $BiFeO_3$ ($R3c$) [50,51] and is attributed to the highly distorted FeO_6 octahedra.

Coming back to the photovoltaic response, it is now necessary to take the anisotropic absorption into consideration. To handle this, the modulated photocurrent is normalized (divided) by the anisotropic absorption. In Fig. 4(f), the photocurrents under a 520-nm laser become almost constant with respect to the light-polarization angle once normalized by the light absorption anisotropy. Similar behavior is also found for white-light illumination (see Fig. S3 within the Supplemental Material [40]). It suggests that, in these two cases, the photocurrents originate mainly from the interface effect, instead of the BPVE. As for 405-nm excitation, experimental data are only well fitted if an

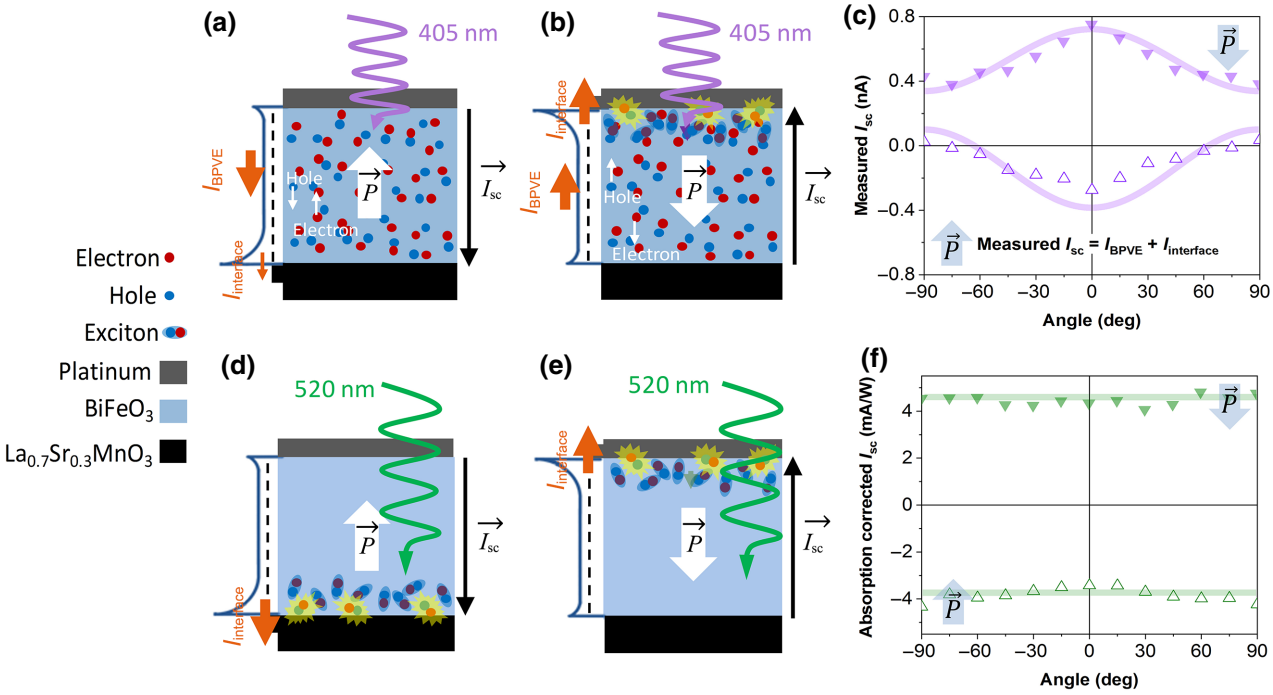

FIG. 4. Crossover between bulk and interface photovoltaic mechanisms. (a) 405-nm laser preferentially generates bulk photovoltaic effects in polarization-up state with negligible current contribution from the interface effect. (b) In the down state, the interface contribution becomes considerable since the top interface is activated and directly exposed to illuminating light. (c) Angle-dependent measured I_{SC} (triangular dots) under 405-nm light fitted by considering combined bulk and interface effects (solid lines). Illumination by 520-nm laser in (d) polarization-up and (e) polarization-down states generate self-trapped excitons in the bulk of $BiFeO_3$; those around the interface are separated by an interfacial built-in field and produce the photocurrent. (f) Angle-dependent I_{SC} (triangular dots) under 520-nm light is almost constant after being normalized by anisotropic absorption.

absorption-modulated interfacial term, $I_{\text{interface}}$, is added to the BPVE current calculated based on Eq. (1). Hence, the total photocurrent under 405 nm light is given by

$$I_{\text{total}}^{405\text{nm}}(\theta) = \pm I_{\text{interface}} \pm 0.15 I_{\text{interface}} \sin\left(2\theta - \frac{\pi}{2}\right) \pm 10^{-10}\left[0.93 + 2.66\sin\left(2\theta + \frac{\pi}{2}\right)\right], \quad (3)$$

where the second term accounts for modulation due to absorption anisotropy, and the negative and positive signs corresponds to polarization-up and -down states, respectively.

The fitted results are shown in Fig. 4(c), where we obtain $I_{\text{Interface}}$ values of -50 pA and $+0.44$ nA for up and down states, respectively. This means the contribution from the interface effect is negligible in the polarization-up state, but becomes considerable in the down state, as indicated by the larger vertical shift of the photocurrent curve to the positive direction. The different interface contribution can be understood by the small absorption depth (approximately 35 nm) at this wavelength (see Fig. S4 within the Supplemental Material [40]). In the polarization-down state, the top interface ($Pt/BiFeO_3$) is activated and directly exposed to light, which allows a strong interface effect [Fig. 4(b)]. In the polarization-up state, the bottom interface ($BiFeO_3/La_{0.7}Sr_{0.3}MnO_3$) is activated, but with little light traveling through the whole film thickness [52], greatly reducing its contribution to the total photocurrent [Fig. 4(a)].

IV. DISCUSSION

The model we propose is consistent with our current understanding on the microscopic origins of the BPVE in noncentrosymmetric materials, namely, ballistic and shift currents. The ballistic photovoltaic current originates from the asymmetric distribution of hot photocarrier momenta in the reciprocal space [53]. By definition, high-energy excitation (405-nm excitation in our case) is needed to provide excess kinetic energy to the photocarriers. The shift current is associated with the shift of electron wave functions in asymmetric media under persistent illumination [54]. First-principles calculations show that transitions involving localized d orbitals exhibit small shift currents [55]. Since the bottom edge of the $BiFeO_3$ conduction band is dominated by the Fe $3d$ states [56,57], band-edge excitation generates self-trapped excitonic states, which are unfavorable for the shift current. Hence, in both mechanisms, 520-nm excitation is unfavorable for producing

a large BPVE current. Nevertheless, the polarization-modulated band-bending field at the interface is efficient in dissociating the self-trapped excitons and results in a sizable photocurrent, which also shows angular modulation due to absorption anisotropy.

V. CONCLUSION

The dominating photovoltaic mechanism in monodomain $BiFeO_3$-based vertical heterostructures depends on the nature of optical excitation. Under high-energy excitation, the (*e*-*h*) pair separation is dominated by the crystal asymmetry of $BiFeO_3$, i.e., the BPVE, in which the interface band-bending-driven photovoltaic effect is still present (which interface matters more depends on the ferroelectric polarization direction, as shown in Fig. 4). On the other hand, the optical structure of $BiFeO_3$ is also characterized by self-trapped *p*-*d* charge-transfer excitons near the absorption edge. These strongly coupled excitons require a strong external field, i.e., band bending at the $BiFeO_3$-metal interface in our devices, to dissociate. Therefore, band-edge excitation leads to an interface-driven photovoltaic response. In this case, the light-polarization-dependent absorption also modulates the photocurrents. Both bulk and interface-driven photovoltaic effects give rise to a sinusoidal dependence on the angle between light polarization and ferroelectric polarization of the sample, but with 90° phase difference, which allows us to distinguish the two effects. These findings help to disentangle the bulk and interface effects and significantly advance our understanding of ferroelectric photovoltaic effects in practical devices.

ACKNOWLEDGMENTS

L.Y. acknowledges startup funds from Soochow University and support from Priority Academic Program Development (PAPD) of Jiangsu Higher Education Institutions. L.Y. also acknowledges support from the National Natural Science Foundation of China (Grants No. 11774249 and 12074278), the Natural Science Foundation of Jiangsu Province (Grant No. BK20171209), and the Key University Science Research Project of Jiangsu Province (Grants No. 18KJA140004 and 20KJA140001). J.W. acknowledges support from the Ministry of Education, Singapore (Grant No. AcRF Tier 1 189/18); a startup grant from the Southern University of Science and Technology (SUSTech), China; and support from the National Natural Science Foundation of China (Grant No. 12074164).

APPENDIX: CALCULATION OF THE PHOTOCURRENT INDUCED BY THE BULK PHOTOVOLTAIC EFFECT

When linearly polarized light is incident on a noncentrosymmetric crystal, the BPVE-generated photocurrent is given by

$$J_i = I_{\text{opt}}\beta_{ijk}e_j e_k, \tag{A1}$$

where I_{opt} is the light intensity (see the Supplemental Material [40] for details), β_{ijk} is a third-rank bulk photovoltaic tensor, and e_j and e_k are projections of the light-polarization vector. In this work, light propagates along z axis to the surface of a monodomain $(001)_{\text{PC}}$-$BiFeO_3$ thin film (space group of $R3c$), giving rise to a photocurrent:

$$J_i = I_o \begin{pmatrix} 0 & 0 & 0 & 0 & \beta_{15} & -\beta_{22} \\ -\beta_{22} & \beta_{22} & 0 & \beta_{15} & 0 & 0 \\ \beta_{31} & \beta_{31} & \beta_{33} & 0 & 0 & 0 \end{pmatrix} \times \begin{pmatrix} e_1^2 \\ e_2^2 \\ 0 \\ 0 \\ 0 \\ 2e_1e_2 \end{pmatrix}. \tag{A2}$$

To be consistent with experimental measurements, the in-plane ferroelectric polarization is taken as a reference. Therefore, the out-of-plane photocurrent can be written as

$$J^{h\upsilon}_{[001]}(\theta) = \frac{I_{\text{opt}}}{3\sqrt{3}}\left[-2\beta_{15} - \sqrt{2}\beta_{22} + 2\beta_{31} + \beta_{33}\right] + \frac{I_{\text{opt}}}{3\sqrt{3}}\left[-2\beta_{15} + 2\sqrt{2}\beta_{22} - \beta_{31} + \beta_{33}\right] \sin\left(2\theta + \frac{\pi}{2}\right), \tag{A3}$$

Similarly, BPVE-induced photocurrents along the $[110]_{\text{PC}}$ and $[\bar{1}10]_{\text{PC}}$ directions can be written as

$$J^{h\upsilon}_{[110]}(\theta) = \frac{I_{\text{opt}}}{3\sqrt{3}}\left[\sqrt{2}\beta_{15} + \beta_{22} + 2\sqrt{2}\beta_{31} + \sqrt{2}\beta_{33}\right] + \frac{I_{\text{opt}}}{3\sqrt{3}}\left[\sqrt{2}\beta_{15} - 2\beta_{22} - \sqrt{2}\beta_{31} + \sqrt{2}\beta_{33}\right] \sin\left(2\theta + \frac{\pi}{2}\right), \tag{A4}$$

$$J^{h\upsilon}_{[\bar{1}10]}(\theta) = I_{\text{opt}}\left[\frac{2}{\sqrt{6}}\beta_{15} + \frac{1}{\sqrt{3}}\beta_{22}\right]\sin(2\theta), \tag{A5}$$

where θ is the angle between light polarization and in-plane ferroelectric polarization, i.e., $[110]_{\text{PC}}$. $J^{h\upsilon}_{[001]}(\theta)$ shows a $\sin[2\theta + (\pi/2)]$ dependence. Moreover, β_{ijk} values are wavelength dependent (Table II).

Experimentally, photocurrents in the $(001)_{\text{PC}}$-$BiFeO_3$ material can be measured along the in-plane polarization direction ($[110]_{\text{PC}}$) and its perpendicular direction

($[\bar{1}10]_{PC}$) by employing a planar configuration. Matsuo *et al.* performed such measurements and obtained the β_{15}, β_{22}, β_{31}, and β_{33} values for 405- and 520-nm lasers [25].

In the vertical configuration and by incorporating the experimental values of β_{15}, β_{22}, β_{31}, and β_{33} (derived from a planar-configuration experiment) into Eq. (A3), the out-of-plane BPVE photocurrents under 405-nm (3.1-eV) and 520-nm (2.4-eV) light are as follows:

$$I_{[001]}^{405\ \mathrm{nm}}(\theta) = -I_{\mathrm{opt}}10^{-10}\left[3.952 + 11.296\ \sin\left(2\theta + \frac{\pi}{2}\right)\right], \tag{A6}$$

$$I_{[001]}^{520\ \mathrm{nm}}(\theta) = -I_{\mathrm{opt}}10^{-11}\left[2.025 + 4.06\ \sin\left(2\theta + \frac{\pi}{2}\right)\right]. \tag{A7}$$

In polarization-up state, I_{SC} is negative at $\theta = 0^{\circ}$ and flips polarity when light polarization is perpendicular to the in-plane ferroelectric polarization. Both 405- and 520-nm-light-induced BPVE photocurrents follow the same trend, but $I_{[001]}^{405\ \mathrm{nm}}$ is 1 order of magnitude larger than that of $I_{[001]}^{520\ \mathrm{nm}}$ for the same light intensity. Furthermore, switching the ferroelectric polarization to the down state changes the sign of β_{ij} and the polarity of the photocurrent.

[1] B. I. Sturman, V. M. Fridkin, and J. Bradley, *The Photovoltaic and Photorefractive Effects in Noncentrosymmetric Materials* (Routledge, London, 2021).

[2] T. Choi, S. Lee, Y. J. Choi, V. Kiryukhin, and S.-W. Cheong, Switchable ferroelectric diode and photovoltaic effect in $BiFeO_3$, Science **324**, 63 (2009).

[3] V. M. Fridkin, *Photoferroelectrics* (Springer Science & Business Media, Berlin, Heidelberg, New York, 2012).

[4] M.-M. Yang, D. J. Kim, and M. Alexe, Flexo-Photovoltaic effect, Science **360**, 904 (2018).

[5] S. Yang, J. Seidel, S. Byrnes, P. Shafer, C.-H. Yang, M. Rossell, P. Yu, Y.-H. Chu, J. Scott, and J. Ager, Above-Bandgap voltages from ferroelectric photovoltaic devices, Nat. Nanotechnol. **5**, 143 (2010).

[6] M. Alexe and D. Hesse, Tip-Enhanced photovoltaic effects in bismuth ferrite, Nat. Commun. **2**, 1 (2011).

[7] A. Bhatnagar, A. R. Chaudhuri, Y. H. Kim, D. Hesse, and M. Alexe, Role of domain walls in the abnormal photovoltaic effect in $BiFeO_3$, Nat. Commun. **4**, 1 (2013).

[8] W. Shockley and H. J. Queisser, Detailed balance limit of efficiency of p-n junction solar cells, J. Appl. Phys. **32**, 510 (1961).

[9] P. Blom, R. Wolf, J. Cillessen, and M. Krijn, Ferroelectric Schottky Diode, Phys. Rev. Lett. **73**, 2107 (1994).

[10] L. Pintilie and M. Alexe, Metal-Ferroelectric-Metal heterostructures with Schottky contacts. I. influence of the ferroelectric properties, J. Appl. Phys. **98**, 124103 (2005).

[11] L. Pintilie, I. Boerasu, M. Gomes, T. Zhao, R. Ramesh, and M. Alexe, Metal-Ferroelectric-Metal structures with Schottky contacts. II. analysis of the experimental current-voltage and capacitance-voltage characteristics of Pb(Zr, Ti)O_3 thin films, J. Appl. Phys. **98**, 124104 (2005).

[12] Z. Tan, L. Hong, Z. Fan, J. Tian, L. Zhang, Y. Jiang, Z. Hou, D. Chen, M. Qin, and M. Zeng, Thinning ferroelectric films for high-efficiency photovoltaics based on the Schottky barrier effect, NPG Asia Mater. **11**, 1 (2019).

[13] R. Guo, L. You, Y. Zhou, Z. S. Lim, X. Zou, L. Chen, R. Ramesh, and J. Wang, Non-Volatile memory based on the ferroelectric photovoltaic effect, Nat. Commun. **4**, 1 (2013).

[14] D. Lee, S. H. Baek, T. H. Kim, J. G. Yoon, C. M. Folkman, C. B. Eom, and T. W. Noh, Polarity control of carrier injection at ferroelectric/metal interfaces for electrically switchable diode and photovoltaic effects, Phys. Rev. B **84**, 125305 (2011).

[15] D. S. Knoche, Y. Yun, N. Ramakrishnegowda, L. Mühlenbein, X. Li, and A. Bhatnagar, Domain and switching control of the bulk photovoltaic effect in epitaxial $BiFeO_3$ thin films, Sci. Rep. **9**, 1 (2019).

[16] J. Seidel, D. Fu, S.-Y. Yang, E. Alarcón-Lladó, J. Wu, R. Ramesh, and J. W. Ager, Efficient Photovoltaic Current Generation at Ferroelectric Domain Walls, Phys. Rev. Lett. **107**, 126805 (2011).

[17] H. Matsuo, Y. Kitanaka, R. Inoue, Y. Noguchi, M. Miyayama, T. Kiguchi, and T. J. Konno, Bulk and domain-wall effects in ferroelectric photovoltaics, Phys. Rev. B **94**, 214111 (2016).

[18] S. Farokhipoor and B. Noheda, Conduction Through 71° Domain Walls in $BiFeO_3$ Thin Films, Phys. Rev. Lett. **107**, 127601 (2011).

[19] Y. Zhou, L. Fang, L. You, P. Ren, L. Wang, and J. Wang, Photovoltaic property of domain engineered epitaxial $BiFeO_3$ films, Appl. Phys. Lett. **105**, 252903 (2014).

[20] V. M. Fridkin, Bulk photovoltaic effect in noncentrosymmetric crystals, Cryst. Rep. **46**, 654 (2001).

[21] H. Festl, P. Hertel, E. Krätzig, and R. V. Baltz, Investigations of the photovoltaic tensor in doped $LiNbO_3$, Phys. Status Solidi B **113**, 157 (1982).

[22] V. M. Fridkin, Parity nonconservation and bulk photovoltaic effect in a crystal without symmetry center, IEEE Trans Ultrason., Ferroelectr. Freq. Control **60**, 1551 (2013).

[23] W. Ji, K. Yao, and Y. C. Liang, Evidence of bulk photovoltaic effect and large tensor coefficient in ferroelectric $BiFeO_3$ thin films, Phys. Rev. B **84**, 094115 (2011).

[24] M.-M. Yang, Z.-D. Luo, D. J. Kim, and M. Alexe, Bulk photovoltaic effect in monodomain $BiFeO_3$ thin films, Appl. Phys. Lett. **110**, 183902 (2017).

[25] H. Matsuo, Y. Noguchi, and M. Miyayama, Gap-State engineering of visible-light-active ferroelectrics for photovoltaic applications, Nat. Commun. **8**, 1 (2017).

[26] R. Nechache, C. Harnagea, S. Li, L. Cardenas, W. Huang, J. Chakrabartty, and F. Rosei, Bandgap tuning of multiferroic oxide solar cells, Nat. Photonics **9**, 61 (2015).

[27] B. Chen, J. Shi, X. Zheng, Y. Zhou, K. Zhu, and S. Priya, Ferroelectric solar cells based on inorganic-organic hybrid perovskites, J. Mater. Chem. A **3**, 7699 (2015).

[28] L. Pintilie, I. Vrejoiu, G. L. Rhun, and M. Alexe, Short-Circuit photocurrent in epitaxial lead zirconate-titanate thin films, J. Appl. Phys. **101**, 064109 (2007).

[29] L. Pintilie, C. Dragoi, and I. Pintilie, Interface controlled photovoltaic effect In epitaxial $Pb(Zr,Ti)O_3$ films with tetragonal structure, J. Appl. Phys. **110**, 044105 (2011).
[30] M. Qin, K. Yao, and Y. C. Liang, Photovoltaic mechanisms in ferroelectric thin films with the effects of the electrodes and interfaces, Appl. Phys. Lett. **95**, 022912 (2009).
[31] W. Ji, K. Yao, and Y. C. Liang, Bulk photovoltaic effect at visible wavelength in epitaxial ferroelectric $BiFeO_3$ thin films, Adv. Mater. **22**, 1763 (2010).
[32] A. Zenkevich, Y. Matveyev, K. Maksimova, R. Gaynutdinov, A. Tolstikhina, and V. Fridkin, Giant bulk photovoltaic effect in thin ferroelectric $BaTiO_3$ films, Phys. Rev. B **90**, 161409 (2014).
[33] J. E. Spanier, V. M. Fridkin, A. M. Rappe, A. R. Akbashev, A. Polemi, Y. Qi, Z. Gu, S. M. Young, C. J. Hawley, and D. Imbrenda, Power conversion efficiency exceeding the shockley–queisser limit in a ferroelectric insulator, Nat. Photonics **10**, 611 (2016).
[34] H. Mai, T. Lu, Q. Sun, R. G. Elliman, F. Kremer, K. Catchpole, Q. Li, Z. Yi, T. J. Frankcombe, and Y. Liu, High performance bulk photovoltaics in narrow-bandgap centrosymmetric ultrathin films, Mater. Horiz. **7**, 898 (2020).
[35] G. Catalan and J. F. Scott, Physics and applications of bismuth ferrite, Adv. Mater. **21**, 2463 (2009).
[36] D. Schmidt, L. You, X. Chi, J. Wang, and A. Rusydi, Anisotropic optical properties of rhombohedral and tetragonal thin film $BiFeO_3$ phases, Phys. Rev. B **92**, 075310 (2015).
[37] S. Choi, H. Yi, S.-W. Cheong, J. Hilfiker, R. France, and A. Norman, Optical anisotropy and charge-transfer transition energies in $BiFeO_3$ from 1.0 to 5.5 eV, Phys. Rev B **83**, 100101 (2011).
[38] C. Tabares-muñoz, J.-P. Rivera, H. Schmid, and Ferroelectric Domains, Birefringence and absorption of single crystals of $BiFeO_3$, Ferroelectrics **55**, 235 (1984).
[39] L. You, F. Zheng, L. Fang, Y. Zhou, L. Z. Tan, Z. Zhang, G. Ma, D. Schmidt, A. Rusydi, and L. Wang, Enhancing ferroelectric photovoltaic effect by polar order engineering, Sci. Adv. **4**, eaat3438 (2018).
[40] See the Supplemental Material at http://link.aps.org/supplemental/10.1103/PhysRevApplied.17.024047 for the coordinate system, Tauc plots, and current-voltage curves of $BiFeO_3$.
[41] R. K. Willardson and A. C. Beer, *Semiconductors and Semimetals* (Academic Press, San Diego, 1977).
[42] J. I. Pankove, *Optical Processes in Semiconductors* (Prentice-Hall, New Jersey, 1971), pp. 92.
[43] R. Pisarev, A. Moskvin, A. Kalashnikova, and T. Rasing, Charge transfer transitions in multiferroic $BiFeO_3$ and related ferrite insulators, Phys. Rev. B **79**, 235128 (2009).
[44] Y. Li, C. Adamo, C. E. Rowland, R. D. Schaller, D. G. Schlom, and D. A. Walko, Nanoscale excitonic photovoltaic mechanism in ferroelectric $BiFeO_3$ thin films, APL Mater. **6**, 084905 (2018).
[45] Y. Yamada, T. Nakamura, S. Yasui, H. Funakubo, and Y. Kanemitsu, Measurement of transient photoabsorption and photocurrent of $BiFeO_3$ thin films: Evidence for long-lived trapped photocarriers, Phys. Rev. B **89**, 035133 (2014).
[46] H. Wen, P. Chen, M. P. Cosgriff, D. A. Walko, J. H. Lee, C. Adamo, R. D. Schaller, J. F. Ihlefeld, E. M. Dufresne, and D. G. Schlom, Electronic Origin of Ultrafast Photoinduced Strain in $BiFeO_3$, Phys. Rev. Lett. **110**, 037601 (2013).
[47] Y. Li, C. Adamo, P. Chen, P. G. Evans, S. M. Nakhmanson, W. Parker, C. E. Rowland, R. D. Schaller, D. G. Schlom, and D. A. Walko, Giant optical enhancement of strain gradient in ferroelectric $BiFeO_3$ thin films and its physical origin, Sci. Rep. **5**, 1 (2015).
[48] Y.-M. Sheu, S. Trugman, Y.-S. Park, S. Lee, H. Yi, S.-W. Cheong, Q. Jia, A. Taylor, and R. Prasankumar, Ultrafast carrier dynamics and radiative recombination in multiferroic $BiFeO_3$, Appl. Phys. Lett. **100**, 242904 (2012).
[49] R. H. Bube, *Photoconductivity of Solids* (RE Krieger Pub. Co., Florida, 1978).
[50] J. K. Shenton, D. R. Bowler, and W. L. Cheah, Influence of crystal structure on charge carrier effective masses in $BiFeO_3$, Phys. Rev. B **100**, 085120 (2019).
[51] C. He, G. Liu, H. Zhao, K. Zhao, Z. Ma, and X. An, Inorganic photovoltaic cells based on $BiFeO_3$: Spontaneous polarization, lattice matching, light polarization and their relationship with photovoltaic performance, Phys. Chem. Chem. Phys. **22**, 8658 (2020).
[52] H. Yi, T. Choi, S. Choi, Y. S. Oh, and S. W. Cheong, Mechanism of the switchable photovoltaic effect in ferroelectric $BiFeO_3$, Adv. Mater. **23**, 3403 (2011).
[53] Z. Dai, A. M. Schankler, L. Gao, L. Z. Tan, and A. M. Rappe, Phonon-Assisted Ballistic Current From First-Principles Calculations, Phys. Rev. Lett. **126**, 177403 (2021).
[54] L. Z. Tan, F. Zheng, S. M. Young, F. Wang, S. Liu, and A. M. Rappe, Shift current bulk photovoltaic effect in polar materials-hybrid and oxide perovskites and beyond, Npj Comp. Mater. **2**, 1 (2016).
[55] S. M. Young and A. M. Rappe, First Principles Calculation of the Shift Current Photovoltaic Effect in Ferroelectrics, Phys. Rev. Lett. **109**, 116601 (2012).
[56] T. Higuchi, Y.-S. Liu, P. Yao, P.-A. Glans, J. Guo, C. Chang, Z. Wu, W. Sakamoto, N. Itoh, and T. Shimura, Electronic structure of multiferroic $BiFeO_3$ by resonant soft X-ray emission spectroscopy, Phys. Rev. B **78**, 085106 (2008).
[57] P. Baettig, C. Ederer, and N. A. Spaldin, First principles study of the multiferroics $BiFeO_3$, Bi_2FeCrO_6, and $BiCrO_3$: Structure, polarization, and magnetic ordering temperature, Phys. Rev. B **72**, 214105 (2005).